Non-steady-state photoelectromotive force in an AlN crystal

M. Bryushinin,[*] V. Kulikov, E. Mokhov, S. Nagalyuk, and I. Sokolov

Ioffe Physical Technical Institute, Politekhnicheskaya 26, 194021 St. Petersburg, Russia

(Received 20 June 2012; revised manuscript received 14 August 2012; published 30 August 2012)

We report the experimental investigation of the non-steady-state photoelectromotive force in aluminum nitride crystal. The sample is illuminated by an oscillating interference pattern formed by two coherent light beams and the alternating current is detected as a response of the material. The experiments are performed for two geometries, where arising photocurrent is parallel or perpendicular to the optical axis of the crystal. Dependencies of the signal amplitude versus light intensity, and temporal and spatial frequencies are measured. The photoelectric parameters of the material are estimated for the light wavelength $\lambda = 532$ nm.

DOI: 10.1103/PhysRevB.86.085209 PACS number(s): 42.65.Sf, 42.70.Nq

I. INTRODUCTION

Aluminum nitride (AlN) stands out against other group III–V compound semiconductors for its large band-gap energy of 6.2 eV. This ensures its utilization in detection of visible and UV light, optical modulators, light-emitting diodes (LEDs), and lasers.[1] Chemical stability, high mechanical hardness (7 in Mohs scale),[2] high melting temperature (3070 K),[3] sufficient thermal conductivity (3.19 W cm^{-1} K^{-1}),[4] and electron mobility (300 cm^2 V^{-1} s^{-1})[5] also promote its application in electronic devices operating in difficult environments.

The AlN crystal has a wurtzite hexagonal structure with unit-cell dimensions $a = 3.111$ Å and $c = 4.980$ Å.[2] The crystal lattice belongs to the 6 mm point symmetry group, which allows the presence of the electro-optic effect in particular. Observation of the photorefractive effect in AlN, i.e., photoinduced change of the refractive index by means of the electro-optic effect, was reported in Ref. 6. The photorefractive holograms recorded in this material demonstrated behavior and characteristics similar to those of "classical" photorefractive crystals ($Bi_{12}SiO_{20}$, $LiNbO_3$).

The photorefractive effect includes the stage of space-charge formation, which occurs via migration of charge carriers, i.e., electric current.[7] This current is the basis of the non-steady-state photoelectromotive force (photo-EMF) effect, which reveals itself as an alternating electric signal arising in the sample illuminated by an oscillating interference pattern.[8,9] Since the current results from the periodic relative shifts of the photoconductivity and space-charge gratings, the technique based on this effect allows determination of the number of photoelectric parameters (conductivity, carrier sign, lifetime, diffusion length, and drift mobility) and can be applied for the investigation of both noncentrosymmetric and centrosymmetric media. In this paper we study the non-steady-state photo-EMF effect in AlN bulk crystal and apply this technique for determination of the photoelectric properties of the material.

II. EXPERIMENTAL SETUP

The experimental arrangement used for the investigation of the non-steady-state photo-EMF in AlN crystal is shown in Fig. 1. The second harmonic of the Nd:YAG laser ($\lambda =$ 532 nm, $P_{\text{out}} \simeq 20$ mW) was split into two beams forming the interference pattern with spatial frequency K and contrast $m = 0.48$ on the sample's surface. The signal beam was phase modulated with frequency ω and amplitude $\delta = 0.62$ by the electro-optic modulator ML-102A. The polarization plane of the light was perpendicular to the incidence plane. The beams were expanded in order to illuminate the whole interelectrode spacing. Two sample orientations were studied with the parallel orientation of the grating vector **K** and the optical c axis [0001] in the former case ("longitudinal" or $\parallel$ geometry), and with the perpendicular orientation in the latter ("transverse" or $\perp$ geometry). The photocurrent arising in the sample generated the corresponding voltage on the load resistor, $R_L = 10$ MΩ. The voltage was amplified and measured using spectrum analyzer SK4-56 (detection bandwidth $\Delta f = 3$ Hz) or the lock-in nanovoltmeter Unipan-232B (with integration time $\tau_{\text{int}} = 1$–100 s). The input resistance of the preamplifier was of 100 MΩ. The sum of the sample and input capacitances was 3 pF. The corresponding correction of the frequency transfer function was performed during calculation of the current amplitude.

The crystal was grown by the physical vapor transport (PVT) technique[10] and had a pale yellow color. The characteristic dimensions of the sample were $6.0 \times 3.8 \times 3.0$ mm^3. The front and back surfaces (3.8×3.0 mm^2) were polished. The silver paste electrodes were painted on the lateral surfaces (6.0×3.0 mm^2 for $\parallel$ geometry and 6.0×3.8 mm^2 for $\perp$ geometry). The static dielectric constant of the material is $\epsilon_\parallel = 9.14$–9.32 and $\epsilon_\perp = 7.76$.[11,12]

III. EXPERIMENTAL RESULTS

The presence of the non-steady-state photo-EMF effect in AlN bulk crystal is the first result which should be pointed out. The amplitude of the detected signal is of order of 0.1–1 pA, which is noticeably lower than that in the model objects—sillenite crystals, $Bi_{12}Si(Ti,Ge)O_{20}$—where it reaches 1 nA.[8] Nevertheless, this amplitude is quite enough for consistent detection of the signal with signal-to-noise ratio of 1–10. The phase of the detected signal indicates that electrons prevail in the process of photo-EMF excitation at low and moderate spatial frequencies of the interference pattern.

We have measured the frequency transfer functions of the non-steady-state photo-EMF signal (Fig. 2) in the longitudinal ($\parallel$) and transverse ($\perp$) geometries of the experiments, i.e., for the cases when the directions of the space-charge field $\mathbf{E}_{\mathbf{SC}}$, grating vector **K**, and photocurrent $\mathbf{J}^\omega$ are parallel or

 ©2012 American Physical Society

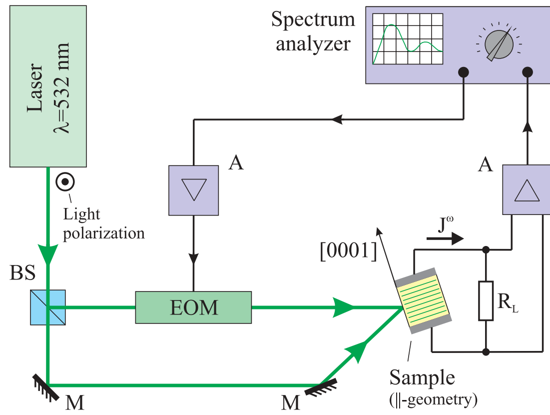

FIG. 1. (Color online) Experimental setup for investigation of the non-steady-state photo-EMF in semiconductors. EOM is the electro-optic modulator, BS is the beam splitter, M are the mirrors, and A are the amplifiers. The axis [0001] is perpendicular to the figure plane for transverse (⊥) geometry.

perpendicular to the c axis. The signal demonstrates typical behavior; namely, there is a linear growth of the amplitude for low frequencies of the phase modulation $\omega < \omega_1$, the frequency-independent region for higher frequencies $\omega_1 < \omega < \omega_2$, and the decay for frequencies $\omega > \omega_2$. These regions are separated by the so-called cutoff frequencies $\omega_1/2\pi = 140$–700 Hz and $\omega_2/2\pi = 13$–30 kHz. These dependencies are well described by the following expression, which is equivalent to that obtained earlier for the simplest model of the semiconductor crystal with one type of partially compensated donor centers:[9]

$$J^{\omega} = J^{\omega}_{m} \frac{i\omega(\omega_2 - \omega_1)}{\omega_1\omega_2 - \omega^2 + i\omega(\omega_2 - \omega_1)}, \quad (1)$$

where J^{ω}_{m} is the current amplitude at the maximum of frequency dependence. The linear growth for low modulation frequencies ($\omega/2\pi < 700$ Hz in Fig. 2) is an important manifestation of the adaptive nature of space-charge formation in wide-gap semiconductor materials. The signal in this frequency region is small since both the space-charge field grating and grating of free carriers (photoconductivity grating) follow the movement of the interference pattern. The spatial shift between the gratings is nearly equal to $\pi/2$, which results in low signal amplitude. For higher modulation frequencies (frequency-independent region) the grating with larger relaxation time can be considered "frozen in," the periodic spatial shifts increase, and the photo-EMF signal reaches its maximum. For very high modulation frequencies ($\omega/2\pi > 13$ kHz in Fig. 2) the oscillation amplitudes of both gratings as well as corresponding relative shifts between them become negligible, and the resulting current vanishes.

The dependence of the signal amplitude versus spatial frequency of the interference pattern, i.e., $J^{\omega}(K)$, is another important characteristic that is usually measured in the non-steady-state photo-EMF experiments (Fig. 3). The behavior of the signal can be easily explained: the signal increases for low K due to the growth of the space-charge field amplitude, which is proportional to the so-called diffusion field $E_D = Kk_BT/e$; the signal decrease for high K results from the diffusion blurring of the conductivity grating. The dependencies were fitted by the following simple expression known from the non-steady-state photo-EMF theory:[8]

$$J^{\omega}(K) \propto \frac{\sigma_0 E_D}{1 + (KL_D)^2}. \quad (2)$$

The diffusion length of electrons was estimated from the measured dependence: $L_{D\parallel} = 0.58$ μm and $L_{D\perp} = 0.92$ μm for the $\parallel$ and $\perp$ geometries, respectively. As seen, the signal amplitude decays faster than K^{-1} and changes its sign for high spatial frequencies. A similar effect was observed earlier in GaAs crystal at $\lambda = 1.15$ μm.[13] Such behavior is explained by the presence of bipolar photoconductivity: the sign of the signal for low spatial frequencies is determined by the carriers with larger photoconductivity, while the carriers with larger generation rate define the sign of the signal for high K. The expression for photo-EMF amplitude can be written in this case as follows:

$$J^{\omega}(K) \propto \frac{\sigma_0^e E_D}{1 + \left(KL_D^e\right)^2} - \frac{\sigma_0^h E_D}{1 + \left(KL_D^h\right)^2}, \quad (3)$$

where $\sigma_0^{e,h}$ and $L_D^{e,h}$ are the average photoconductivities and diffusion lengths of electrons and holes, respectively. One can note that this expression fits experimental dependencies much

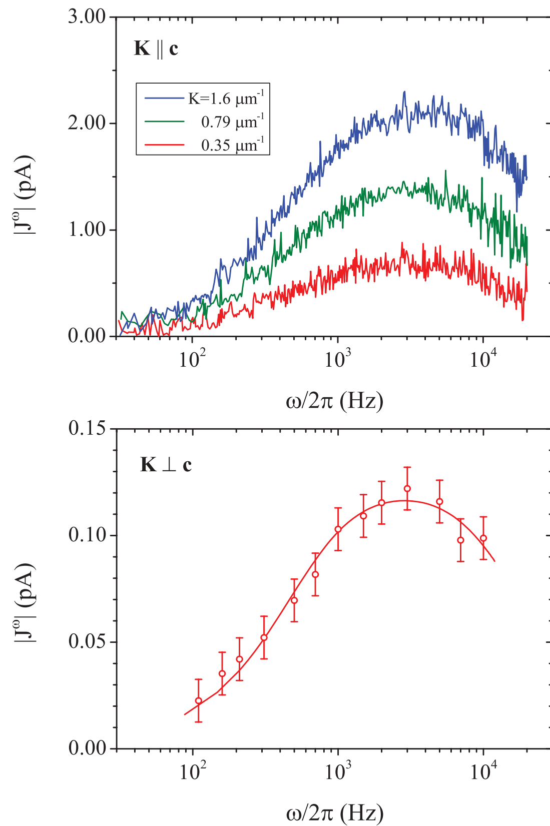

FIG. 2. (Color online) Frequency transfer functions of the non-steady-state photo-EMF signal in AlN crystal. The dependences are measured for two geometries: (top) $\mathbf{K} \parallel c$ axis, $K = 0.35$ μm^{-1}, 0.79 μm^{-1}, 1.6 μm^{-1}, and (bottom) $\mathbf{K} \perp c$ axis, $K = 2.0$ μm^{-1}. $I_0 = 110$ mW/cm^2. The solid line shows approximation by Eq. (1) with $\omega_1/2\pi = 600$ Hz and $\omega_2/2\pi = 14$ kHz.

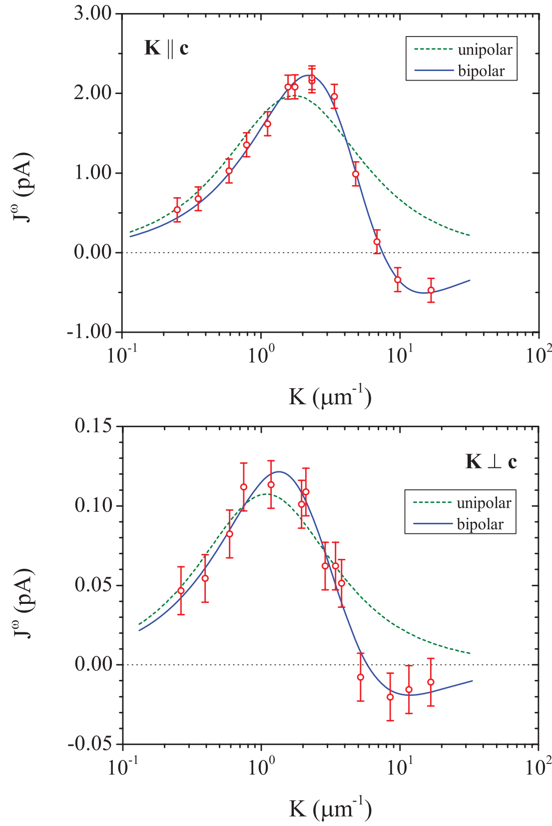

FIG. 3. (Color online) Dependence of the non-steady-state photo-EMF amplitude on the spatial frequency of the interference pattern. The dependencies are measured for two geometries: (top) $\mathbf{K} \parallel c$ axis and (bottom) $\mathbf{K} \perp c$ axis. $I_0 = 110\ \mathrm{mW/cm^2}$. Dotted and solid lines show approximation by Eqs. (2) and (3), respectively.

better (Fig. 3), and it describes the change of the signal sign. The best fit was obtained for the following combination of material parameters: $\sigma^e_{0\parallel}/\sigma^h_{0\parallel} = 1.8$, $L^e_{D\parallel} = 0.27\ \mu\mathrm{m}$, $L^h_{D\parallel} = 0.18\ \mu\mathrm{m}$ for $\parallel$ geometry and $\sigma^e_{0\perp}/\sigma^h_{0\perp} = 5.3$, $L^e_{D\perp} = 0.58\ \mu\mathrm{m}$, $L^h_{D\perp} = 0.20\ \mu\mathrm{m}$ for $\perp$ geometry.

Dependencies $\omega_1(K)$ and $\omega_2(K)$ measured in $\parallel$ geometry are presented in Fig. 4. The expressions for the cutoff frequencies obtained earlier for the simplest model of semiconductor with one type of compensated donor centers are as follows:[9]

$$\omega_1 \simeq \left[\tau + \tau_M\left(1 + K^2 L_D^2\right)\right]^{-1}, \tag{4}$$

$$\omega_2 = \omega_1 + \tau_M^{-1} + \left(1 + K^2 L_D^2\right)\tau^{-1}. \tag{5}$$

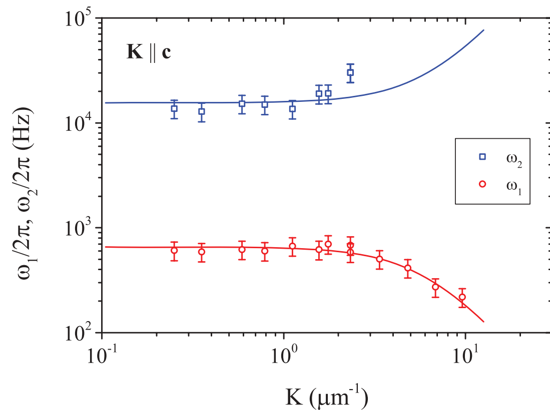

FIG. 4. (Color online) Dependencies of the first ω_1 and second ω_2 cutoff frequencies on the spatial frequency of the interference pattern. $I_0 = 110\ \mathrm{mW/cm^2}$. Solid lines show the approximation by Eqs. (4) and (5).

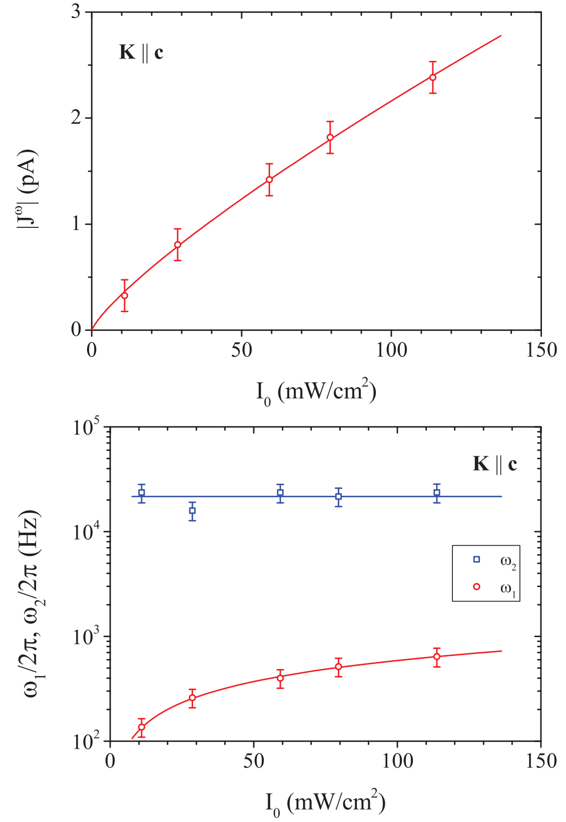

FIG. 5. (Color online) Dependencies of the non-steady-state photo-EMF amplitude (top) and cutoff frequencies (bottom) versus average light intensity. $\mathbf{K} \parallel c$ axis, $K = 1.9\ \mu\mathrm{m}^{-1}$.

The following parameters were determined from the experimental dependencies: $\tau_{M\parallel} = 0.23$ ms, $\tau_\parallel = 11\ \mu$s, and $L_{D\parallel} = 0.17\ \mu$m. Using the measured value of the Maxwell relaxation time $\tau_M = \epsilon\epsilon_0/\sigma_0$ one can easily estimate the average conductivity σ_0 of the material. For the sample in $\parallel$ geometry it equals $\sigma_{0\parallel} = 3.6 \times 10^{-9}\ \Omega^{-1}\ \mathrm{cm}^{-1}$.

Characteristic relaxation times $\tau_{M\perp}$ and $\tau_\perp$ for $\perp$ geometry were also estimated from the only transfer function shown in Fig. 2: $\tau_{M\perp} \simeq 0.26$ ms, $\tau_\perp \simeq 12\ \mu$s. The corresponding photoconductivity equals $\sigma_{0\perp} \simeq 2.6 \times 10^{-9}\ \Omega^{-1}\ \mathrm{cm}^{-1}$.

Dependence of the non-steady-state photo-EMF versus average light intensity was studied as well (Fig. 5). Nonlinear growth of the first cutoff frequency and signal amplitude in the maximum of the transfer function was observed: $\omega_1 \propto I_0^{0.67}$ and $J^\omega \propto I_0^{0.81}$. These results correlate with the nonlinearity of holographic recording in AlN,[6] although the powers of function I^x are different. The second cutoff frequency remains nearly constant, which means the conductivity relaxation time is independent of light intensity.

IV. DISCUSSION

The experiments on non-steady-state photo-EMF excitation have revealed strong anisotropy of the AlN crystal: the photocurrent density along the c axis is about 25 times higher than the one across the c axis. In the frames of unipolar conductivity this result can be attributed solely to anisotropy of the photoconductivity, since $j^{\omega} \propto \sigma_0 E_D$, while the diffusion field $E_D \propto K$ remains comparable for both orientations. In the frames of bipolar conductivity the photo-EMF amplitude is the difference of the electron and hole parts: $j^{\omega} \propto (\sigma_0^e C^e - \sigma_0^h C^h) E_D$, where $C^{e,h}$ are the coefficients taking into account the diffusion blurring of conductivity grating [see Eq. (3)]. Thus the discussed anisotropy can be attributed to both the absolute values σ_0^e, σ_0^h and their relation σ_0^e/σ_0^h.

There is a serious contradiction in the experimental data and theoretical approach used. As it was mentioned above, the current along the c axis is higher that that in the transverse direction (Fig. 3), whereas dependence $J_{\perp}^{\omega}(K)$ seems to be shifted to lower spatial frequencies with respect to dependence $J_{\parallel}^{\omega}(K)$. Intuitively the opposite shift is expected, since the larger current amplitude in the direction of the c axis implies the larger photoconductivities, larger $\mu\tau$ products, and larger diffusion lengths. Quantitatively we can describe this contradiction as follows. The photocurrent amplitude for low K can be written as $j^{\omega}(K) \propto (\sigma_0^e - \sigma_0^h) E_D$. Then the ratio of signals along and across the c axis is represented as

$$\frac{j_{\parallel}^{\omega}}{j_{\perp}^{\omega}} = \left(\frac{L_{D\parallel}^h}{L_{D\perp}^h}\right)^2 \frac{\sigma_{0\parallel}^e/\sigma_{0\parallel}^h - 1}{\sigma_{0\perp}^e/\sigma_{0\perp}^h - 1}. \tag{6}$$

Here we assumed the generation rates of electrons and holes to be independent of light polarization. After substitution of the material parameters estimated from Fig. 3 we obtain $j_{\parallel}^{\omega}/j_{\perp}^{\omega} = 0.15$; i.e., the calculated photocurrent along the c axis is not higher but lower than that across the c axis. Now we cannot explain this contradiction, we can just speculate with the possible polarization dependence of the generation rates mentioned above. The relative errors in determination of material parameters are of the order of 10% and result mainly from the instability of the laser's output power.

The previous studies[2,14,15] of charge transport in undoped AlN provided a rather wide range for the dark conductivity: $\sigma_d = 10^{-12}$–$10^{-9}\ \Omega^{-1}\ \mathrm{cm}^{-1}$. In this work we obtained the conductivity values of the order of $10^{-9}\ \Omega^{-1}\ \mathrm{cm}^{-1}$ as well. Since the noticeable growth of the first cutoff frequency versus light intensity was revealed (Fig. 5), we can state that photoconductivity exceeds the dark conductivity, and the space-charge field grating is recorded effectively for the used illumination wavelength and power level. We can also roughly estimate the mobility of carriers using the obtained values of diffusion lengths L_D and lifetimes τ. For electrons, which dominate in photo-EMF excitation, we obtain $\mu_{\parallel}^e \sim 3 \times 10^{-3}\ \mathrm{cm}^2\ \mathrm{V}^{-1}\ \mathrm{s}^{-1}$ and $\mu_{\perp}^e \sim 1 \times 10^{-2}\ \mathrm{cm}^2\ \mathrm{V}^{-1}\ \mathrm{s}^{-1}$. These values are sufficiently smaller than those calculated ($300\ \mathrm{cm}^2\ \mathrm{V}^{-1}\ \mathrm{s}^{-1}$) and measured ($125\ \mathrm{cm}^2\ \mathrm{V}^{-1}\ \mathrm{s}^{-1}$) earlier.[5,16] Such difference is often attributed to the trapping processes, which can reduce the average velocity of charge migration (and corresponding effective mobility) by several orders.

Nonlinear photoconductivity ($\sigma_0 \propto \omega_1 \propto I_0^{0.67}$) along with intensity-independent relaxation time [$\tau \propto \omega_2 = \mathrm{const}(I_0)$] give rise to some contradiction in the frames of the simplest model of a unipolar semiconductor: nonlinear photoconductivity is usually accompanied by the change of relaxation time. In the case of a bipolar semiconductor the relative contributions of electrons and holes to the overall conductivity and its relaxation time can change with the light intensity and this discrepancy may not be significant.

Generally speaking, the bipolar conductivity of AlN crystal is unexpected in itself. The energy of photons is 2.3 eV, whereas the band gap of the material is 6.2 eV. This means that electrons and holes cannot be generated from the same local levels. There must be at least two groups of levels in the forbidden gap providing extrinsic absorption of the green light and corresponding independent generation of electrons and holes.

V. CONCLUSION

To summarize we studied the effect of non-steady-state photo-EMF in photosensitive material—aluminum nitride bulk crystal. The significant anisotropy of the material was revealed in the experiments with excitation of the photo-EMF along and across the [0001] axis. The presence of the bipolar photoconductivity was established from the change of the signal sign for high spatial frequencies. The average photoconductivity of the material was estimated from the measurements of the signal amplitude versus frequency of phase modulation. The dependence of the signal versus spatial frequency provided the estimation of the diffusion lengths of electrons and holes.

The obtained results have demonstrated that the non-steady-state photo-EMF technique can be considered a powerful tool for investigation of wide-band-gap semiconductors. A number of photoelectric parameters are estimated using the only arrangement. In contrast to the standard methods of semiconductor characterization the technological problem of Ohmic contacts for high-resistive materials is not so significant here, since the effect of the non-steady-state photo-EMF is based on the excitation of an alternating current.

ACKNOWLEDGMENTS

The financial support from the Ministry of Knowledge Economy of Korea is gratefully acknowledged.

*mb@mail.ioffe.ru

[1] Y. Taniyasu, M. Kasu, and T. Makimoto, Nature (London) **441**, 325 (2006).
[2] K. Taylor and C. Lenie, J. Electrochem. Soc. **107**, 308 (1960).
[3] V. Vinogradov, A. Kostanovskii, and A. Kirillin, High Temp. High Pressures **23**, 685 (1991).

[4] G. Slack, R. Tanzilli, R. Pohl, and J. Vandersande, J. Phys. Chem. Solids **48**, 641 (1987).
[5] V. Chin, T. Tansley, and T. Osotchan, J. Appl. Phys. **75**, 7365 (1994).
[6] T. Nagai, R. Fujimura, T. Shimura, and K. Kuroda, Opt. Lett. **35**, 2136 (2010).
[7] M. Petrov, S. Stepanov, and A. Khomenko, *Photorefractive Crystals in Coherent Optical Systems* (Springer-Verlag, Berlin, 1991).
[8] M. Petrov, I. Sokolov, S. Stepanov, and G. Trofimov, J. Appl. Phys. **68**, 2216 (1990).
[9] I. Sokolov and S. Stepanov, J. Opt. Soc. Am. B **10**, 1483 (1993).
[10] E. Mokhov, O. Avdeev, I. Barash, T. Chemekova, A. Roenkov, A. Segal, A. Wolfson, Y. Makarov, M. Ramm, and H. Helava, J. Cryst. Growth **281**, 93 (2005).
[11] A. Collins, E. Lightowlers, and P. Dean, Phys. Rev. **158**, 833 (1967).
[12] W. Moore, J. Freitas, R. Holm, O. Kovalenkov, and V. Dmitriev, Appl. Phys. Lett. **86**, 141912 (2005).
[13] S. Stepanov and G. Trofimov, Sov. Phys. Solid State **31**, 49 (1989).
[14] J. Edwards, K. Kawabe, G. Stevens, and R. Tredgold, Solid State Commun. **3**, 99 (1965).
[15] R. Francis and W. Worrell, J. Electrochem. Soc. **123**, 430 (1976).
[16] Y. Taniyasu, M. Kasu, and T. Makimoto, Appl. Phys. Lett. **85**, 4672 (2004).